Biomedicine & Pharmacotherapy 177 (2024) 116991

Contents lists available at ScienceDirect

Biomedicine & Pharmacotherapy

journal homepage: www.elsevier.com/locate/biopha

Novel selective inhibitors of macropinocytosis-dependent growth in pancreatic ductal carcinoma

Silvia Brambillasca [a,*,1], Maria Rosaria Cera [a,1], Adrian Andronache [a], Sumit Kumar Dey [b,2], Giovanni Fagá [a,3], Daniele Fancelli [a], Emanuela Frittoli [b], Maurizio Pasi [a,4], Michela Robusto [a], Mario Varasi [a], Giorgio Scita [b,c,**], Ciro Mercurio [a,*]

[a] Experimental Therapeutics Program, IFOM ETS, the AIRC Institute of Molecular Oncology, Milan, Italy
[b] IFOM ETS, the AIRC Institute of Molecular Oncology, Milan, Italy
[c] Department of Oncology and Haemato-Oncology, University of Milan, Milan, Italy

ARTICLE INFO

Keywords:
Macropinocytosis
Pancreatic ductal adenocarcinoma (PDAC)
Drug screening
Drug repurposing
FDA-approved drugs

Chemical compounds studied in this article:
Pyrvinium Pamoate (PubChem CID: 54680693)
Ivermectin (PubChem CID: 6321424)
Tyrphostin A9 (PubChem CID: 5614)
LY2090314 (PubChem CID: 10029385)

ABSTRACT

Macropinocytosis is a cellular process that enables cells to engulf extracellular material, such as nutrients, growth factors, and even whole cells. It is involved in several physiological functions as well as pathological conditions. In cancer cells, macropinocytosis plays a crucial role in promoting tumor growth and survival under nutrient-limited conditions. In particular *KRAS* mutations have been identified as main drivers of macropinocytosis in pancreatic, breast, and non-small cell lung cancers. We performed a high-content screening to identify inhibitors of macropinocytosis in pancreatic ductal adenocarcinoma (PDAC)-derived cells, aiming to prevent nutrient scavenging of PDAC tumors. The screening campaign was conducted in a well-known pancreatic *KRAS*-mutated cell line (MIAPaCa-2) cultured under nutrient deprivation and using FITC-dextran to precisely quantify macropinocytosis. We assembled a collection of 3584 small molecules, including drugs approved by the Food and Drug Administration (FDA), drug-like molecules against molecular targets, kinase-targeted compounds, and molecules designed to hamper protein-protein interactions. We identified 28 molecules that inhibited macropinocytosis, with potency ranging from 0.4 to 29.9 μM (EC_{50}). A few of them interfered with other endocytic pathways, while 11 compounds did not and were therefore considered specific "bona fide" macropinocytosis inhibitors and further characterized. Four compounds (Ivermectin, Tyrphostin A9, LY2090314, and Pyrvinium Pamoate) selectively hampered nutrient scavenging in *KRAS*-mutated cancer cells. Their ability to impair albumin-dependent proliferation was replicated both in different 2D cell culture systems and 3D organotypic models.

These findings provide a new set of compounds specifically targeting macropinocytosis, which could have therapeutic applications in cancer and infectious diseases.

1. Introduction

Macropinocytosis is a clathrin-independent endocytic mechanism that allows the internalization of extracellular fluid, macromolecules, and necrotic debris into eukaryotic cells through large vesicles known as 'macropinosomes' [1]. This process involves the remodeling of the actin

Abbreviations: **APH**, Acid Phosphatase Assay; **BSA**, Bovine Serum Albumin; **CAFs**, Cancer Associated Fibroblasts; **CME**, Clathrin-Mediated Endocytosis; **DAPI**, 4′,6-diamidino-2-phenylindole; **EGFR**, Epidermal Growth Factor Receptor; **EIPA**, 5-N-ethyl-N-isopropyl amiloride; **FITC**, Fluorescein Isothiocyanate; **GSK3**, Glycogen Synthase kinase 3; **LDH**, Lactate Dehydrogenase; **PDAC**, Pancreatic Ductal Adeno Carcinoma; **PDGFR**, Platelet-Derived Growth Factor Receptor; **PTEN**, Phosphatase and Tensin Homolog; **WNT**, Wingless/Integrated.

* Corresponding authors.
** Corresponding author at: IFOM ETS, the AIRC Institute of Molecular Oncology, Milan, Italy.
E-mail addresses: silvia.brambillasca@ifom.eu (S. Brambillasca), giorgio.scita@ifom.eu (G. Scita), ciro.mercurio@ifom.eu (C. Mercurio).
[1] These authors contributed equally
[2] Present address: Memorial Sloan Kettering Cancer Center, New York, USA
[3] Present address: Human Technopole, Milan, Italy.
[4] Present address: Fondazione I.R.C.C.S. Policlinico San Matteo, Pavia, Italy.

https://doi.org/10.1016/j.biopha.2024.116991
Received 7 March 2024; Received in revised form 12 June 2024; Accepted 15 June 2024
Available online 21 June 2024

cytoskeleton, which promotes the extension of membrane ruffles leading to the formation of a macropinocytic cup. Subsequent closure of this cup marks its internalization into the cell as a fluid-filled vesicle, known as a macropinosome. Macropinosomes range from 0.2 to 5 μm in size and are significantly larger than endosomes originated by coated vesicles, whose average size is 0.1 μm [2]. Upon formation, macropinosomes can fuse back with plasma membrane releasing their content to extracellular space, or they can fuse with lysosomes, resulting in the formation of highly degradative organelles. In these latter structures, engulfed macromolecules, such as albumin, extracellular matrix proteins, and necrotic cell debris, are broken down into their constituent building blocks, which can fuel biosynthetic processes or adenosine triphosphate (ATP) generation [3].

In mammalian cells, macropinocytosis is involved in diverse physiological processes with a specific role in innate and adaptive immunity, migration, infection, and pathological conditions such as atherosclerosis, renal dysfunction, and neurodegenerative diseases [4,5]. More recently, macropinocytosis has been directly implicated in cell metabolism and shown to play a key role in various solid cancers, including pancreatic, lung, prostate, colon, bladder, breast, and brain cancer [6,7]. In these malignancies, it acts as a nutrient-scavenging pathway that allows tumor cells to meet their increased nutrient demands and sustain cell survival and proliferation even under the nutrient-poor conditions of the tumor microenvironment [8,9]. Consistent with this metabolic function, macropinocytosis has been shown to confer resistance to drugs targeting cancer anabolism [10] and to mammalian Target Of Rapamycin (mTOR) inhibition in pancreatic cancer cells [11]. These latter tumoral cells were specifically shown to utilize Nuclear factor erythroid 2-Related Factor 2 (NRF2)-induced macropinocytosis as an alternative nutrient pathway to escape autophagy inhibition [12]. Additionally, macropinocytosis has been associated with Yes-associated protein 1 (YAP) and transcriptional co-activator with PDZ-binding motif (TAZ) (YAP/TAZ)-driven epithelial-mesenchymal transition and shown to impact the metastatic potential of tumor cells [13].

In keeping with the critical role of macropinocytosis in tumor cell metabolism, both oncogenic variants and tumor suppressor mutations have been shown to promote the process [6,14]. For example, *KRAS*-induced macropinocytosis has been shown to play a critical role in PDAC, non-small cell lung cancer, and breast cancer [8,10]. In other tumors instead, such as bladder and brain tumors, including glioblastoma and neuroblastoma [15,16], *HRAS* mutations are the main drivers. Several studies also highlighted a link between the activation of the *vSrc* oncogene and macropinocytosis in different cell types [17,18]. Additionally, mutations of *P3IKCA* leading to hyperactivation of Phosphatidylinositol 3-kinase (PI3K) or the loss of Phosphatase and Tensin Homolog (PTEN) can also promote constitutive macropinocytosis in breast cancer and prostate carcinoma [9,10]. Besides RAS and PTEN signaling, other pathways can regulate macropinocytosis, including the canonical Wingless/Integrated (WNT) pathway in colon cancer [19,20]; the YAP/TAZ mechanosignaling routes in pancreatic cancer [13]; and the Epidermal Growth Factor-Receptor (EGFR)/p21-Activated Kinases (PAK) axis in a subset of pancreatic cancer cells [21].

All these observations indicate that several oncogenic mechanisms directly or indirectly impinge onto the macropinocytic machinery, suggesting that this process is specifically selected for and promotes tumorigenesis.

Among the different cancer types that exploit macropinocytosis, PDAC is a particularly prominent case. PDACs represent a major unmet clinical need as they are generally detected only at a late stage with a dismal prognosis. They are genetically and phenotypically heterogeneous and associated with a pervasive desmoplastic reaction that fuels cancer progression but also causes nutritional starvation that forces the tumor cells to rewire and reprogram their metabolic strategies [22–24]. Among these adaptive metabolic strategies, increased macropinocytosis has emerged as an alternative mechanism adopted by PDAC in both primary human cancer cells [25] and murine models [8,26] to scavenge proteinaceous and lipid materials that sustain cancer growth under nutritionally-deprived conditions. Therefore, strategies to curb macropinocytosis are expected to be effective in preventing metabolic adaptation and cancer growth, specifically in this tumor type.

The lack of potent and selective macropinocytosis inhibitors, the relevance of this mechanism for the survival of pancreatic cancer cells, and the need to identify novel and effective treatments for pancreatic cancer, prompted us to conduct a high-content screening for the identification of novel and more effective macropinocytosis inhibitors.

In this study, we present the identification and characterization of novel and selective inhibitors of macropinocytosis in pancreatic ductal adenocarcinoma cell lines. We specifically selected these compounds based on their ability to potently inhibit the uptake of the classical macropinocytosis cargo, 70kD dextran, without affecting other endocytic pathways. These small molecules demonstrated a selective ability to halt growth that was supported by albumin internalization and catabolism under conditions of nutrient deprivation in macropinocytic-proficient cancer cells. Importantly, we observed this effect not only in 2D cell culture conditions but also in a more physiological and relevant model of multicellular epithelial pancreatic spheroids, which were formed in the presence of cancer-associated fibroblasts (CAFs).

2. Materials and methods

2.1. Cell culture

BxPC3 and MDA-MB-231 cell lines were obtained from ATCC, MIAPaCa-2 from Istituto Zooprofilattico Sperimentale della Lombardia e dell'Emilia Romagna (IZSLER, Italy), PANC-1 from ECACC; all lines were maintained under 5 % CO_2 at 37C in medium supplemented with 10 % FBS, 2 mM glutamine, 25 mM HEPES and 1 % penicillin/streptomycin (Pen/Strep). MIAPaCa-2, PANC-1 and MDA-MB-231 cell lines were cultured in DMEM (Gibco), while BxPC-3 in RPMI 1640 (EuroClone). MIAPaCa-2 cells constitutively expressing Histone H2B-EGFP were used for 3D-spheroid formation; this reporter cells line was generated by retroviral infection of MIAPaCa-2 cells with pBABE- puro-EGFP-H2B vector. CAF8 cells were purchased from Vitro Biopharma (#CAF08) and cultured in MSC-Gro™ low serum maintaining medium (Vitro Biopharma #PC00B5) according to manufacturer's instructions. All cells were tested negative for mycoplasma contamination before experiments.

2.2. Reagents

Library for the primary screening campaign was assembled starting from collections of different vendors: FDA-approved and drug-like molecules were from Selleck Chemicals, Sigma-Aldrich and MicroSource; kinase-targeted molecules were from Asinex, Enamine, BioFocus, ChemBridge and Chem-X; targeting protein-protein interaction molecules were from Asinex. Small molecules selected for further characterization were repurchased from Sigma-Aldrich (Tyrphostin A9 #T182, LY2090314 #SML1438), MedChemExpress (Ivermectin #HY-15310) and Selleck Chemicals (Pyrvinium Pamoate #S5816). Reference compounds included in screening were obtained from Sigma-Aldrich (EIPA #A3085, Chlorpromazine #C8138) and Abcam (Dynole 34–2 #ab120463). Additionally, FITC-Dextran (# D1822) and Alexa633-hTRSF (#T23362) were purchased from Invitrogen; BSA-FAF (Fraction V, fatty acid free, #A8806), DAPI (#D9542) and Mowiol mounting media (#81381) were from Sigma-Aldrich; paraformaldehyde 4 % in PBS was from HiMedia (#TCL119).

2.3. Screening compound plates preparation

All operations and liquid handling were performed on Microlab STAR Workstation (ML-STAR, Hamilton). Compounds were arrayed at 10 mM in DMSO, according to final layout, in 384-well PCR barcoded

plates (ThermoScientific, #BC-1384) with the 1000ul-pipetting channels; a 2-points serial dilution 1:5 in DMSO was performed in separate 384-plates with the 96-well head. Each 384-plate accommodated 256 small molecules as single replicate and remaining wells were dedicated to positive and negative controls (15 mM EIPA and 100 % DMSO respectively). A total of 42 compound plates were prepared, sealed and stored at 4℃ until the day of assay, when 3ul were transferred to 97ul of serum- and glutamine-free medium in temporary plates (384-well plates Euroclone, #GR781080); 5ul of pre-diluted compounds were finally dispensed in corresponding wells on assay plates (PhenoPlate 384-well PerkinElmer, #6057300) with cells maintained in 25ul under nutrient deprivation conditions (see below).

For dose-response characterization of dextran uptake, the selected compounds were manually arrayed in columns 3–4 and 13–14 in 384-well PCR plates, either at 10 mM or 6 mM in DMSO; EIPA was also present in few positions at 15 mM, as well as 100 % DMSO, respectively as positive and negative controls; a 4-points serial dilution 1:4 in DMSO was performed with ML-STAR. All compounds were tested in triplicate on separate plates, with pre-dilution in medium and addition to assay plates as described above.

For Transferrin uptake assay, the selected compounds were manually dispensed in columns 2–3–4 in V-bottom 96-well storage plate (ThermoFisher Scientific, #AB-1058), each in DMSO at 200x the concentration to be tested on cells; Dynole at 1 mM and 100 % DMSO were included in few wells respectively as positive and negative controls; EIPA and Chlorpromazine were also present at 6 mM as reference compounds. 3ul of each compound were automatically transferred to 97ul of medium in a 384-well temporary plate and subsequently 5ul were dispensed on 25ul cells. Each compound was tested in triplicate inside the same assay plate.

2.4. Dextran and Transferrin uptake assay

Cells were seeded with ML-STAR (3000 cells/well) in PhenoPlate 384-well, in 50ul DMEM with 4 % FBS, 0.5 mM glutamine, 25 mM HEPES, 1 % Pen/Strep, and automatically moved to the workstation integrated incubator (Cytomat 2 C-Lin, ThermoScientific). Nearly 30 hours after seeding 40ul of medium were removed with 96-well head and replaced with 15ul of basal medium (DMEM, 25 mM HEPES, 1 % Pen/Strep) to allow for 18 h incubation in nutrient deprivation conditions; 5ul of drugs pre-diluted to 6x final concentration in basal medium were added to cells for 3 hours (0.5 % DMSO final on cells) before addition for an extra hour of 10ul FITC-dextran 0.8 mg/ml in basal medium; assay plates were always returned to the incubator after each reagent addition. Alternatively, for human Transferrin uptake assay, drugs were incubated for 30 minutes and then 10ul of Alexa633-hTRSF 30 ug/ml in basal medium were added and incubated for 5 min at 37℃ on the Multiflex Heating module on the ML-STAR deck. FITC-dextran/Alexa633-hTRSF incorporation was blocked by washing the cells twice with 100ul ice-cold PBS and twice with 100ul ice-cold acid buffer (50 mM glycine in PBS, pH 2.5) using the Wellwash Versa plate washer (ThermoFisher Scientific). Cells were then fixed for 25 min with 4 % paraformaldehyde and subsequently stained for 10 min with DAPI (0.2 ug/ml in PBS), both dispensed with the Multidrop Combi reagent dispenser (ThermoFisher Scientific). Plates were lastly washed twice with 100ul PBS before being sealed and stored at 4℃ for imaging.

2.5. Macropinosomes visualization and quantification

Images were acquired with a 40x/0.6 NA dry objective on Operetta CLS high-content system (PerkinElmer) equipped with an Andor Zyla 5.5 camera, sampling 8 fields per well. Images acquired via Harmony 4.9 were transferred to Columbus platform (PerkinElmer, v2.9.1) and analyzed with a customized image analysis pipeline: cell boundaries were segmented on Digital Phase Contrast channel after identification of DAPI-stained nuclei; cells with saturated signal in DAPI or FITC channel, or with markedly reduced area compared to average cell dimensions were excluded from further analysis; background in FITC channel was subtracted with a sliding parabola function, then single spots were identified inside the cell area and filtered at first for dimension (selecting those with an area of 0.2–20.0 μm^2, corresponding to a diameter of 0.5–5.0μm), then by brightness (selecting spots with signal intensity 2.5 fold above the noise of cellular autofluorescence signal); several parameters were obtained for each identified cell and then averaged as median value for each well, such as cell and nuclear area, size and intensity of dextran spots, number of spots per cell (SpotNumber), spots per cell area unit (SpotDensity), percentage of cell area occupied by spots (PercentSpotArea). SpotDensity was used as the primary endpoint in the screen.

2.6. Screening data analysis

The set of morphological and physiological parameters estimated in Columbus went through a custom data management system that fully integrates compounds library management, sample tracking/handling and data annotation/registration. As such, the set of parameters of every single well of all assay plates were associated to corresponding experimental treatments and conditions. The annotated data went then through a custom pipeline for standard high-throughput screening statistical data analysis implemented in Matlab (MathWorks). For every estimated parameter, plate-wise data were first pre-processed to remove possible systematic spatial effects using a surface determined by regression (MLE) to interpolate the Negative Controls Samples data. Data of all plates passing the Quality Control step (Z-factors > 0.5 between Negative and Positive Controls) went further to intra-plate normalization to define Percent Inhibition. Candidate hits were selected based on robust z-scores estimated on median-absolute-deviations of normalized values on selected parameters (Number of Spots per Cell, Spots Density, and Percent Spots Area per Cell Area).

2.7. Albumin growth-rescue experiments

Cells were plated in 96-well plate at a density of 1500–3000 cells per well in complete DMEM medium. 30 hours after seeding cells were rinsed with PBS and incubated with compounds under exam at different doses in starvation conditions (DMEM, 2.5 % dialyzed FBS, 0.1 mM glutamine, 25 mM HEPES) in the presence of 4 % BSA-FAF (Bovine Serum Albumin-Fatty Acid Free); control conditions with 50uM EIPA and vehicle-only in starvation ±BSA supplementation were always present, to allow for drug inhibitory effect normalization. Cell number was evaluated at the beginning (T0, DMSO control only) and after 96 h of treatment: cells were fixed for 15 minutes at room temperature with 4 % paraformaldehyde, DAPI-stained and images were taken with a 20x/0.4 NA dry objective on Operetta CLS (PerkinElmer), covering approximately 90 % of each well area; cell nuclei were counted for each well in Columbus (PerkinElmer, v2.9.1) excluding pyknotic nuclei and dying cells; data were then normalized to the nuclei number of control wells for each plate, as specified in figure legends.

2.8. Spheroids generation and treatment

Spheroids were generated by co-culturing MIAPaCa-2 tumor cells with pancreatic Cancer Activated Fibroblasts (CAF8). The cells were seeded in a ratio 1:2 (3300 tumor cells and 6600 CAF cells) in Ultra Low Attachment/Round-bottom 96-well plates (Costar, #7007) and incubated for 4 days until spheroid formation. Spheroids were then rinsed twice with 100ul PBS (by centrifuging the plates for 2 minutes at 50rcf with low break) before addition of compounds in 100ul starvation medium (DMEM, 2.5 % dialyzed serum, glutamine-free) supplemented or not with 4 % BSA-FAF. Viability and cytotoxicity were assessed after 6 days of treatment. Spheroids viability was measured with Acid Phosphatase (APH) Assay, following procedures described previously [27].

Briefly, spheroids were washed twice with 100ul PBS in 96-well plate and resuspended in 100ul of buffer containing 0.1 M sodium acetate pH 5.0, 1 % Triton X-100 and 2 mg/ml p-nitrophenyl phosphate (SigmaAldrich, #N4645); plates were incubated at 37C for 90 minutes, the reaction stopped by addition of 10ul 1 N NaOH and the absorbance measured at 405 nm using the EnVision XCite plate reader (PerkinElmer). Spheroids cytotoxicity was assessed with LDH-Glo Cytotoxicity Assay (Promega, #J2380) according to manufacturer's instructions. Briefly, 5ul of culture medium were diluted 1:80 in LDH Storage Buffer (200 mM Tris-HCl pH 7.3, 10 % Glycerol, 1 % BSA); an equal volume of LDH Detection Reagent was then added to 12.5ul diluted sample in a 384-white-plate (Greiner, #781075) and incubated for 60 minutes at room temperature before recording luminescence signal on EnVision XCite plate reader (PerkinElmer). Images were acquired with an air 5x/0.16 NA objective on Operetta CLS high-content system (PerkinElmer). Z-stacks of 7 focal planes with 30um step size were acquired from each field via Harmony 4.9. The acquired images were transferred to Columbus platform and maximum intensity projection was generated for EGFP signal analysis: the total spheroid area was segmented in the brightfield channel and total EGFP intensity was quantified after background subtraction.

2.9. Interference RNA-mediated knockdown experiments

MIAPaCa-2 cells were reverse transfected with 50 nM SignalSilence siRNA oligos with Lipofectamine RNAiMAX reagent (ThermoFisher Scientific, #13778150) according to manufacturer's instructions, seeding cells in 6-well plate with or without fibronectin-coated glass coverslip; SignalSilence siRNA oligos were from Cell Signaling Technologies (GSK3α/β: #6301; control: #6568). Cells were analyzed 72 h upon transfection, after an overnight incubation with starvation medium (1 % FBS, 0.1 mM glutamine): wells with coverslip were used for dextran uptake assay, while the remaining ones for evaluation of interference efficiency by qRT-PCR. FITC-dextran was added to cells for 30 min at 37C, at a final concentration of 1 mg/ml; uptake was blocked by rinsing four times with cold PBS, cells immediately fixed for 10 min with 4 % paraformaldehyde and stained with 0.2 ug/ml DAPI in PBS, before mounting coverslips on slides with Mowiol mounting media. Images were taken with a 60x oil immersion objective on CSU Olympus inverted confocal microscope equipped with an Andor iXon Ultra 897 camera, sampling minimum 12 fields per specimen. For gene expression analysis, total RNA was isolated from cells with RNeasy Mini kit (QIAGEN) according to manufacturer's instruction; 1 ug of purified RNA was retrotranscribed with ImProm-II Reverse Transcription System (Promega); 5 ng of cDNA was analyzed in triplicates with the TaqMan Gene expression Assay (Thermofisher) on the 7500 Real-Time PCR System (Thermofisher). GSK3α and GSK3β transcript levels were normalized to the housekeeping gene GAPDH and expressed as CNRQ (Calibrated Normalized Relative Quantity). Primer assay IDs were: GSKα, Hs00997938_m1; GSKβ, Hs001047719_m1; GAPDH, Hs99999905_m1.

2.10. Statistical analysis

Prism9 (GraphPad) software was used for data analysis and graphic representations, except for the analysis of screening dataset that were performed with MatLab. Data are expressed as mean ± standard deviation (SD) or standard error of the mean (SEM) for minimum $n \geq 3$ biological replicates, as indicated in figure legends. The EC_{50} for dose-response inhibition of dextran uptake was calculated in MatLab using nonlinear regression curve fit. Comparisons of mean values were performed with unpaired two-tailed Student's *t*-test or one-way ANOVA with Bonferroni's post hoc test, as specified in figure legends; *p<0.05, **p<0.01, *** p<0.001, ****p<0.0001.

3. Results

3.1. Identification of small molecule inhibitors of dextran internalization

To identify small molecules that inhibit macropinocytosis, we conducted a High-Content Screening using a compound collection of 3584 small molecules assembled in-house. This library contains 989 FDA-approved drugs, 1328 drug-like molecules against defined molecular targets, 1024 compounds belonging to a kinase-targeted library, and 243 compounds defined as molecules designed to hamper protein-protein interactions.

High-molecular weight dextran uptake from the extracellular medium represents the mainstay and a well-established assay to monitor and measure macropinocytosis in normal and cancer cells [28]. Accordingly, we optimized a cell-based assay in 384-well plate allowing us to quantify the extent of macropinocytosis in pancreatic adenocarcinoma cells (MIAPaCa-2) under conditions mimicking tumor nutrient deprivation. FITC-dextran (70 kDa) was used as a molecular probe to quantify various macropinocytosis parameters, with 5-(N-ethyl--N-isopropyl) amiloride (EIPA), a widely-used and characterized macropinocytosis inhibitor that targets Na^{++}-proton pumps [29], as the positive control [8,30]. We conducted the primary screening with small molecules at three different doses (2, 10, and 50 μM). Each 384-well plate included vehicle (DMSO)-treated cells as a basal dextran uptake control, and EIPA-treated cells as a positive control of uptake inhibition (Fig. 1A -representative images).

We performed the screening in human MIAPaCa-2 cells, which are homozygous for the K-Ras^{G12C} allele [31]. They have been shown to display appreciably higher levels of dextran uptake, particularly after nutrient starvation [8], compared to pancreatic ductal carcinoma cells like BxPC3 cells, which express wild-type K-Ras. MIAPaCa-2 cells seeded in 384-well plates were cultured in nutrient deprivation conditions (1.5 % serum and 0.2 mM glutamine) for 18 hours before addition of the various compounds. FITC-dextran was finally added in the last hour of incubation in the presence of small molecules. The cells were extensively washed and stained with diamidino-2-phenylindole (DAPI) to detect nuclei and processed by immunofluorescence to reveal FITC-dextran internalization. We implemented an automatic, operator-independent imaging pipeline to detect and quantify Dextran-positive macropinosomes over an average of about 600 cells per experimental condition. The automatic image analysis pipeline determines various parameters, including cell number, number of macropinosomes per cell (Spot number) and per cell area unit (Spot density), and percentage of cell area occupied by spots (% Spot area). Compounds reducing cell number by more than 70 % were marked as cytotoxic and excluded from the analysis. Among these compounds are molecules that robustly inhibit cell adhesion, thereby resulting in the loss of cells during the washing steps. An average robust Z′ factor of ≥0.5 was determined for all the analyzed parameters and a Z-score transformation was used as a hit calling metric. We defined as positive inhibitory hits the compounds that downregulated spot density at least two of the three tested doses with a robust z-score ≥3 (Fig. 1B). On basis of this criteria, and after removing compounds interfering with the assay readout due to intrinsic fluorescence, we identified 32 small molecule inhibitors (hit rate of 0.89 %).

Next, we conducted a confirmation round by testing the selected candidates in triplicate at three different doses (2,10, and 50 μM). Following the same criteria used in the primary screening, 28 out of 32 compounds were validated as macropinocytic inhibitors with an overall hit confirmation rate of 87.5 %. We also validated five small molecules that induced, rather than abrogated, the uptake of dextran (robust z-score<-3 at all doses), such as Digoxin, Colchicine, Levobunolol, Proscillaridin, and a kinase-targeted compound. Finally, we narrowed down inhibitory compounds to 18, selecting those inhibiting dextran uptake with a z-score ≥3 at the lowest dose (2μM). These 18 molecules were considered "bona fide" macropinocytosis inhibitors (Figure S1, marked with magenta star).

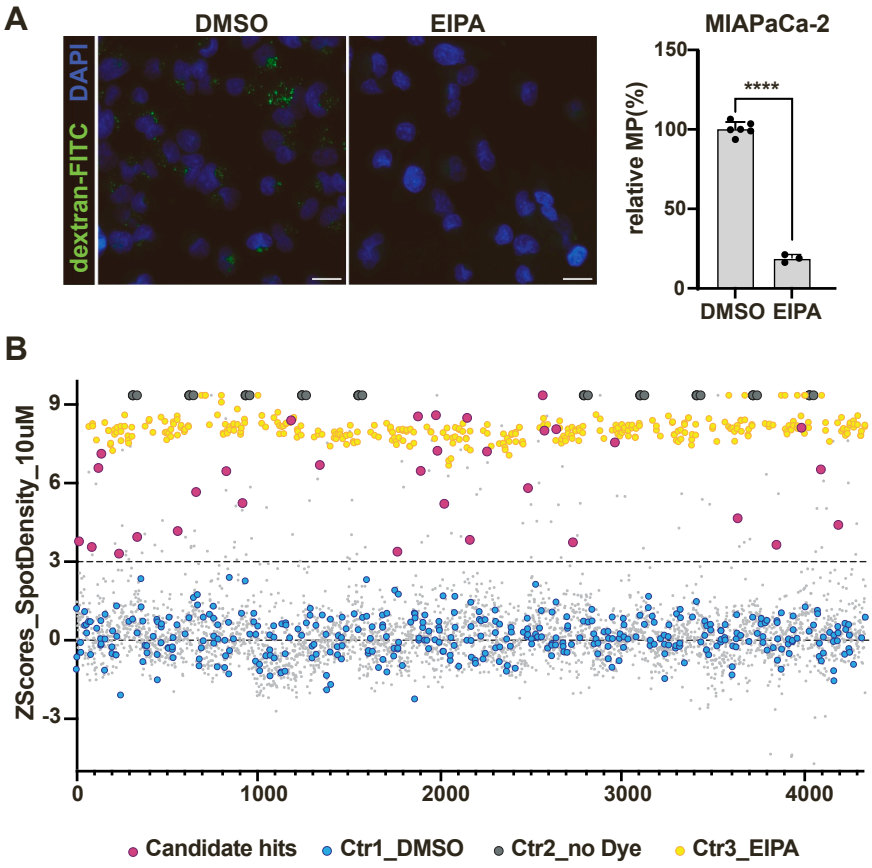

Fig. 1. : Identification of new macropinocytosis inhibitors from a library of bioactive compounds.(A) Representative images of macropinocytosis uptake in MIAPaCa-2 cells, in control conditions (DMSO: negative control; EIPA: positive control, 75uM). Dextran-FITC was used as a marker of macropinosomes. Scale bar: 20 μm. Quantification of macropinocytosis as described in (A), relative to the values of DMSO negative control (as SpotDensity parameter); data are reported as mean ± SD for n=6 (DMSO) or n=3 (EIPA) biological replicates with at least 600 cells scored per condition; ****p≤0.0001 by unpaired two-tailed Student's *t*-test. MP= macropinocytosis. (B) Results distribution from primary screening, depicting SpotDensity parameter at 10uM of compound; each spot represents the activity of a single compound, reported as z-score after normalization on negative (DMSO, light blue) and positive control (no dye, grey); 75uM EIPA was included in all plates as additional positive control (yellow); highlighted as candidate hits (magenta) are compounds scoring above the threshold (z-score=3) also at 2uM and/or 50uM.

3.2. EC_{50} determination of selected macropinocytic inhibitors

To better define the potency of the validated and selected inhibitors we determined their EC_{50}. To this end, serial dilutions of the compounds at concentrations ranging from 50 to 0.19 μM or from 30 to 0.12 μM were incubated with MIAPaCa-2 cells under primary screening conditions. The different concentration ranges were required because a few compounds displayed intrinsic fluorescence that interfered with the assay measurements. Absolute EC_{50} values were calculated from logarithmic plots of the inhibitor concentrations versus the percentage of dextran uptake relative to the vehicle-treated controls (Fig. 2). Absolute EC_{50} values ranged from 0.4 to 29.9 μM. It is of note that the majority of identified compounds were significantly and robustly more effective than EIPA. Several of the most potent compounds belonged to the kinase targeted subgroup, with unknown target, while five compounds were approved drugs. These include the multi tyrosine kinase inhibitor Bosutinib, already approved for cancer therapy; the anthelmintics Pyrvinium Pamoate and Fenbendazole; the antibiotic Gramicidin S; the JAK2/FLT-3/IRAK1 inhibitor Pacritinib recently approved for myelofibrosis treatment [32]. Noticeably, Fenbendazole is structurally similar to Flubendazole, a molecule that was previously identified as a putative macropinocytosis inhibitor in a screening conducted to identify inhibitors of PhorbolMyristate-Acetate-induced macropinocytosis on macrophages [33]. AvermectinA1 belongs to a family of macrocyclic lactones with antiparasitic activity, among which Ivermectin is the most commonly used and was approved as a drug nearly forty years ago.

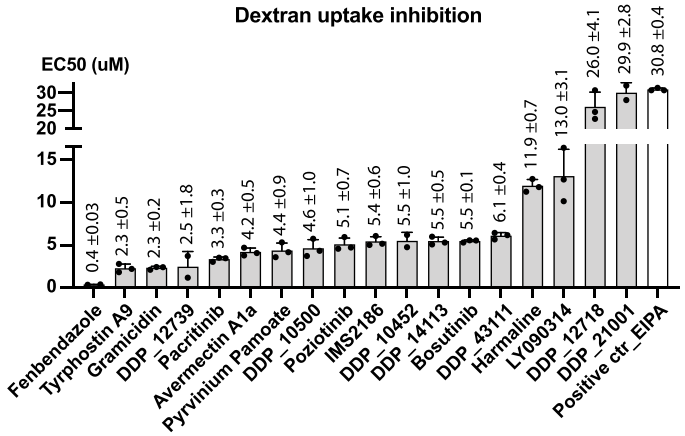

Fig. 2. : Inhibition efficacy of selected macropinocytosis inhibitors. EC_{50} values were determined via dextran uptake assay in MIAPaCa-2 cells, following SpotDensity parameter. Dose-response curves were obtained plotting inhibitors activity as percentage of dextran uptake relative to the DMSO control; the effect of EIPA is reported as a reference (white bar). EC_{50} values are reported as mean ± SD, n=3 biological replicates (n=2 for Fenbendazole, DDP_12739, DDP_10452 and DDP_21001).

Poziotinib is a pan-epidermal growth factor receptor inhibitor that had shown promising results in patients with Non-Small Cell Lung cancer and breast cancer [34,35].

3.3. Selected inhibitors specifically impair macropinocytosis, but not Clathrin-mediated endocytosis

Our main scope was the identification of selective macropinocytosis inhibitors. Hence, to determine the specificity of the confirmed hits, we evaluated their effects on the internalization of fluorescent Transferrin, a ligand for the transferrin receptor that enters exclusively via Clathrin-mediated endocytosis (CME) [36]. For this specific screening, we exploited Dynole and Chlorpromazine, two well-characterized CME inhibitors [37,38], as positive controls. Selected macropinocytic compounds were tested at doses corresponding to their absolute EC_{50} values in the dextran uptake assay. The near-complete abrogation of transferrin uptake determined by Dynole and Chlorpromazine treatments validated the assay. Importantly, EIPA did not affect transferrin incorporation (Fig. 3A and B). Several compounds inhibited transferrin uptake to varying degrees, whereas several others did not or inhibited the transferrin uptake by less than 15 % (Fig. 3A). Thus, compounds in the former group were considered dual macropinocytosis and CME inhibitors, while those in the latter were selective macropinocytosis inhibitors.

3.4. Selected macropinocytic inhibitors impair albumin-dependent PDAC cell growth under nutritional limited conditions

Macropinocytosis is a process that enables cancer cells to scavenge for nutrients, which they can internalize and catabolize to derive amino acids that support cancer cell growth [25]. Serum albumin is a highly abundant protein found in both blood plasma and extracellular fluid in mammals. Research indicates that cancer cells can utilize macropinocytosis to consume albumin, deriving amino acids that facilitate cancer cell growth in nutrient-deprived conditions [8,39]. Specifically, the albumin rescue effect has been observed in MIAPaCa-2 cells when glutamine is lacking, and this process is shown to be reliant on proficient macropinocytosis. The administration of EIPA, which impairs macropinocytosis, has been found to prevent the rescue of growth [8]. Hence, we tested the impact of the selected and specific macropinocytic inhibitors on the growth of cancer cells under nutrient-deprived conditions that recapitulate the conditions occurring in the tumor microenvironment, when tumor cells become addicted to scavenging mechanisms [8].

We initially confirmed that a reduction in glutamine and serum led to impaired cell growth in MIAPaCa-2 cells with macropinocytotic ability. However, when these cells were cultured in the presence of albumin at physiological levels, their proliferation increased significantly. Crucially, this effect was prevented by EIPA treatment. Conversely, albumin supplementation failed to reverse growth impairment in non-macropinocytic cells like BxPC-3 [8] (as seen in Fig. 4A).

After identifying macropinocytosis inhibitors, we investigated their potential to block albumin rescue, similarly to what observed with EIPA treatment. For this purpose, we carried out initial experiments to establish the optimal dosage range for each compound when used in the albumin rescue assay. We then compared the differential effect on growth rescue between MIAPaCa-2 and BxPC-3 cells at the selected

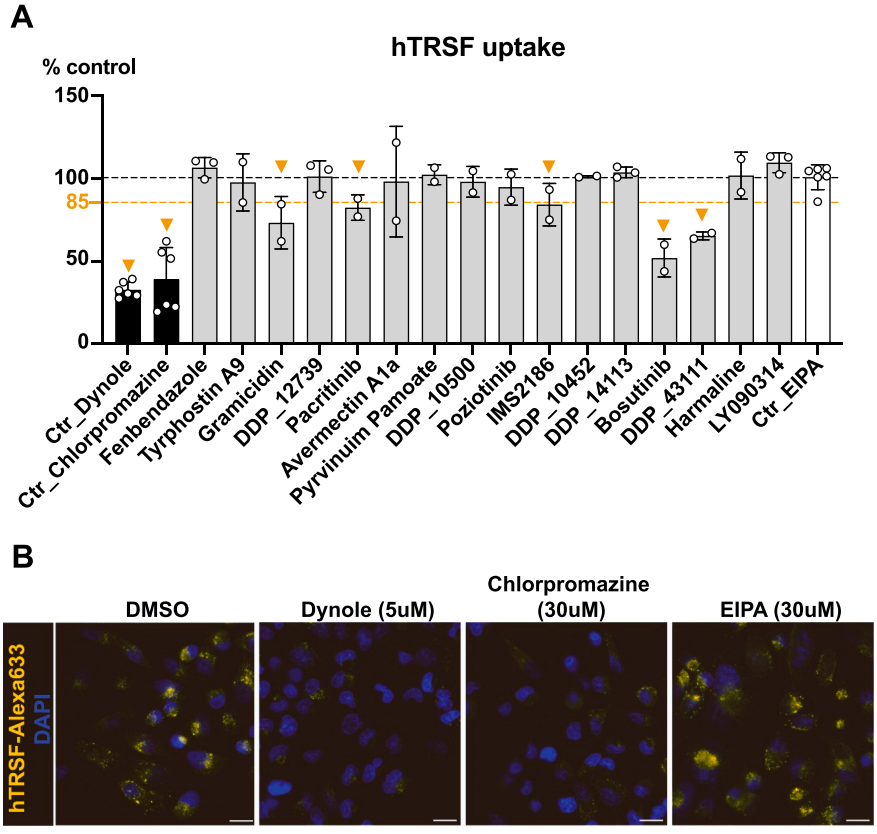

Fig. 3. : Selectivity of identified inhibitors. (A) Effect of selected inhibitors on clathrin-mediated endocytosis. MIAPaCa-2 cells were challenged with the indicated inhibitors (each at their EC_{50}) and the extent of human Transferrin-Alexa633 internalization was obtained by image analysis upon microscopy imaging; the quantified CellMeanSignal for each compound was reported relative to the vehicle-treated control (DMSO). Dynole and Chlorpromazine were included as positive controls of Clathrin-mediated endocytosis inhibition (black bars); EIPA was included as negative control (white bar). Yellow arrowheads highlight compounds inhibiting more than 15 % the Transferrin uptake. Data are presented as mean ± SD; n=6 (Dynole, Chlorpromazine, EIPA), n=3 (Fenbendazole, DDP_12739, DDP_14113 and LY090314), n=2 (all remaining compounds) as biological replicates, with at least 450 cells scored per condition. (B) Representative images of human-Transferrin uptake assay described in (A); hTRSF-Alxa633 intracellular signal was quantified for each cell. Scale bar: 20 μm.

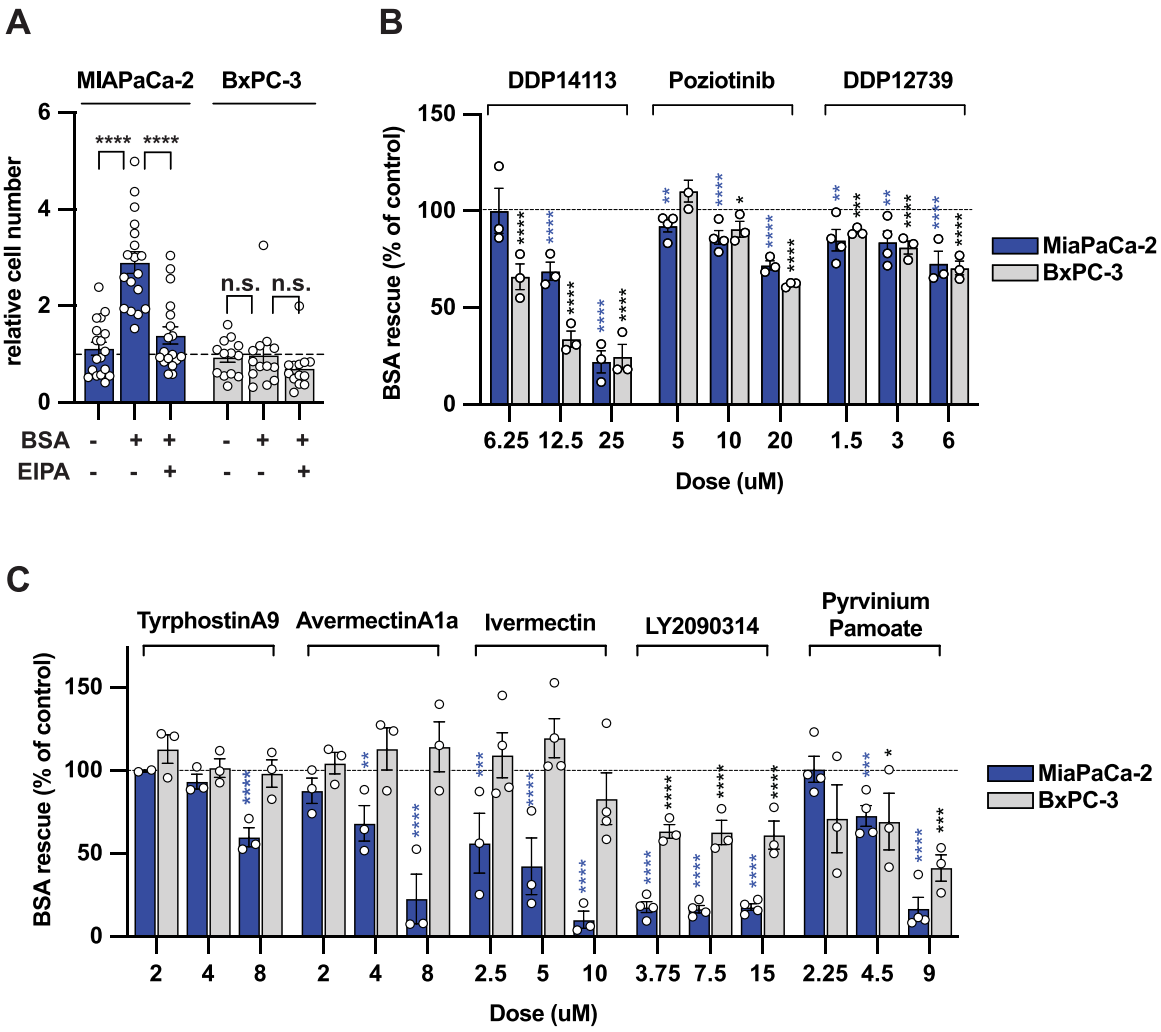

Fig. 4. : Inhibitors impairment of BSA-dependent proliferation in nutrient-limiting conditions. (A) Proliferation of MIAPaCa-2 and BxPC-3 cells (respectively blue and grey) after 96 h of growth in starvation conditions (low serum/low glutamine) ± 4 % BSA and EIPA (50uM). Data are reported as relative to the cell number at the beginning of starvation, on the day after seeding. Values are mean ± SEM of n≥11 independent experiments performed in triplicates. (B) Effect of inhibitors on BSA-dependent proliferation during starvation, in MIAPaCa-2 and BxPC-3 cell lines (blue and grey, respectively). Data are expressed as percentage of growth after 96 h compared to DMSO-treated cells in starvation +4 % BSA. These compounds showed equal activity between the two cell lines. (C) Differential activity of inhibitors in MIAPaCa-2 versus BxPC-3 cells, experimental conditions as described in (B). In all panels, where not differently indicated, values are mean ±SEM of n≥3 independent experiments performed in triplicates. *p≤0.05, **p≤0.01, ***p≤0.001, ****p≤0.0001 by one-way ANOVA with Bonferroni post-hoc test; multiple comparisons for each cell line and each inhibitor performed separately, relative to DMSO control; n.s., not significant.

doses. Seven out of the eleven tested compounds significantly reduced the albumin rescue effect in MIAPaCa-2 cells (as shown in Fig. 4B and C), while others showed no effect (as shown in Figure S2A). Three of the seven active compounds had a similar impact on the growth of non-macropinocytic cells BxPC-3 (Fig. 4B). Importantly, under the same experimental conditions, four of the seven highlighted compounds did not interfere with BxPC-3 proliferation, or did so to a lesser extent compared to MIAPaCa-2 cells (as shown in Fig. 4C and Table S1). These compounds were Tyrphostin A9, AvermectinA1a, LY2090314, and Pyrvinium Pamoate. AvermectinA1a was not commercially available for repurchasing, so we also included Ivermectin in the panel of screened compounds. Ivermectin is a widely used antiparasitic drug and a close analog of AvermectinA1a. Ivermectin was found to be as effective as AvermectinA1a in the albumin rescue assay in MIAPaCa-2 cells without affecting BxPC-3 cells. Therefore, Ivermectin was used in subsequent experiments. The structures of the compounds that showed biological activity in MIAPaCa-2 cells, including Ivermectin, are depicted in Fig. 5.

Prompted by these findings, we explored if the four chosen compounds could also suppress macropinocytosis in other macropinocytic cell types, such as PANC-1, a cell line exhibiting epithelial morphology that was isolated from the pancreatic duct of a patient with epithelioid carcinoma, and also the triple-negative breast cancer line, MDA-MB-231 [10,21]. Both cell lines exhibited significant macropinocytosis, which was reduced by EIPA as shown in Fig. 6A. We then conducted a dose-response test for the four compounds to evaluate their capacity to hinder dextran uptake and macropinocytosis in these varied cell lines. As shown in Fig. 6B, all four compounds were effective in inhibiting dextran uptake in these cells, confirming their ability to inhibit macropinocytosis beyond MIAPaCa-2 cells. Furthermore, we found that these same compounds prevented the effect of albumin supplementation in PANC-1 cells grown under nutrient starvation conditions. These outcomes suggest that the identified compounds are selectively potent against various macropinocytic cancer cells, albeit with varying efficacy levels, as depicted in Fig. 7A and B.

Intriguingly, among the compounds that inhibited both macropinocytosis and the albumin growth effect, one was identified as a Glycogen Synthase Kinase 3 (GSK3) inhibitor. This was particularly noteworthy because previous data, such as those from Albrecht et al. (2020) [40], suggested that inhibiting GSK3 might actually stimulate, rather than suppress, macropinocytosis in certain contexts, specifically

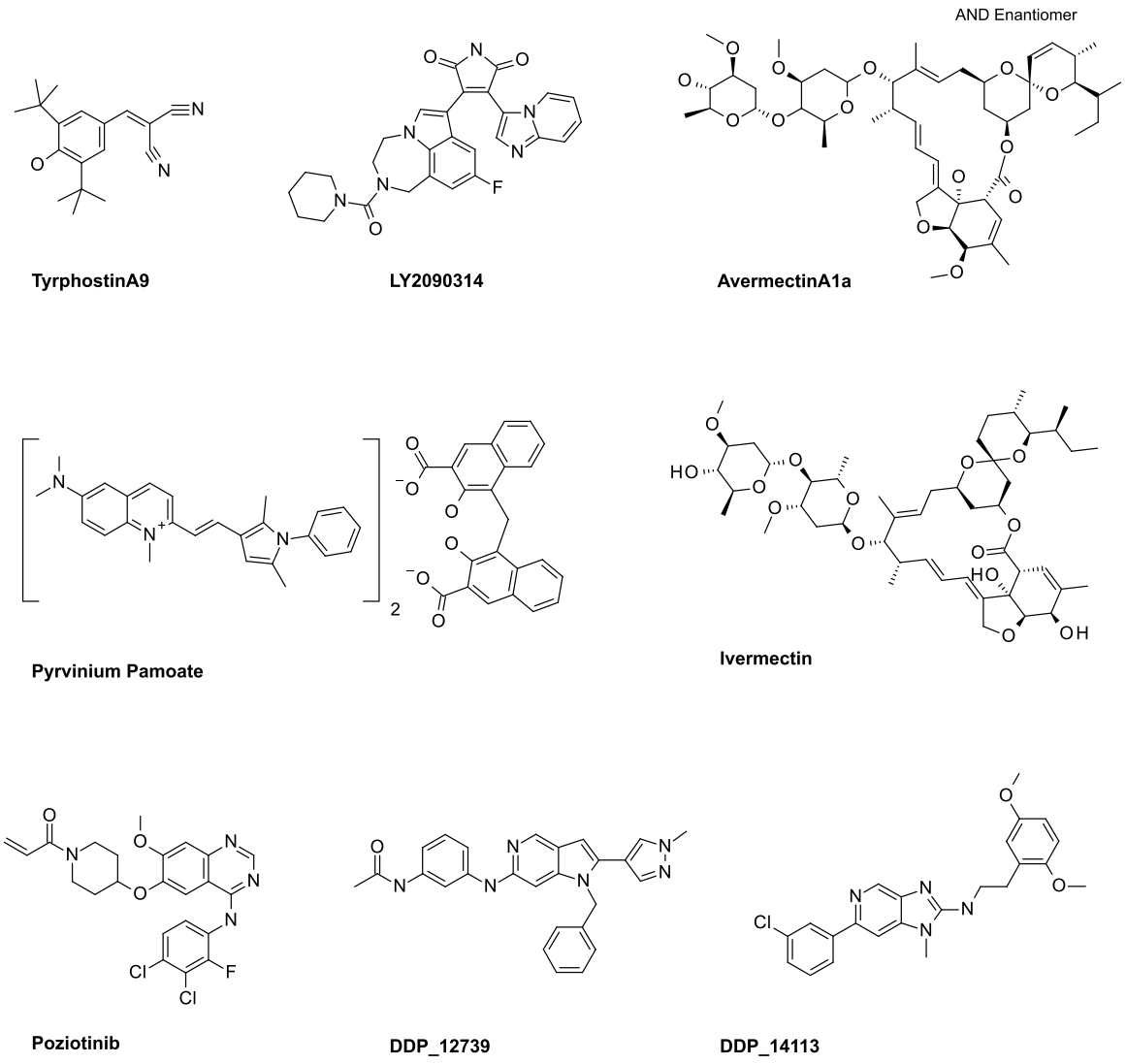

Fig. 5. Chemical structures of selected compounds showing activity on MIAPaCa-2 cells.

in the absence of WNT in a particular hepatocellular carcinoma cell line. This led us to further investigate the role of GSK3 in macropinocytosis within our cell model. We found that upon siRNA-mediated silencing of both alpha and beta isoforms of GSK3 kinase, there was a marked reduction in dextran uptake in MIAPaCa-2 cells rather than an increase (as shown in Fig. 8A and B), validating the on-target effect of the identified compound.

3.5. The selected macropinocytic inhibitors impact the growth of organotypic 3D culture of MIAPaCa-2 and cancer associated fibroblasts

Finally, we assessed the impact of four selected macropinocytic inhibitors on the albumin rescue assay using a 3D model containing both MIAPaCa-2 adenocarcinoma pancreatic cancer cells and pancreatic cancer-associated and activated fibroblasts (CAFs). When cultured in ultra-low attachment plates, MIAPaCa-2 cells formed loose cell aggregates, while co-culture with CAFs promoted the formation of more compact spheroids (Fig. 9A), as previously observed [41]. Supplementation with physiological levels of albumin rescued spheroid growth once shifted to starvation conditions, as determined by cell vitality evaluation using the Acid Phosphatase Assay (APH) (Fig. 9B) [27].

To evaluate the effectiveness of the inhibitors, we tested them at doses three times higher than those effective in the 2D Albumin Rescue Assay, based on observations for EIPA, which required a high dose to achieve a similar effect. Our results showed that EIPA treatment abrogated the albumin-dependent benefit and induced cell death, as detected by an increase in Lactate Dehydrogenase (LDH) protein release (Fig. 9C). Similarly, all the compounds except for Ivermectin significantly reduced the advantage of albumin supplementation and induced cell death. The morphology of the spheroids at the end of treatment reflected these effects. All compounds, except for Ivermectin, slightly reduced the size of the spheroids, making them appear more compact compared to the untreated controls. In contrast, spheroids treated with Ivermectin exhibited cellular outgrowths spreading from the core, similar to those seen in the vehicle-treated condition (Fig. 9D). Interestingly, at the same time all the tested drugs showed an inhibitory effect on the cancer cell component within the spheroids, whose identity could be assessed by the expression of a constitutive EGFP-marker (Fig. 9D, FITC/BF overlay and EGFP signal quantification).

4. Discussion

Macropinocytosis is a non-selective endocytic process that generates peculiar large vesicles through which cells can uptake and assimilate extracellular fluids and diverse macromolecules such as albumin, extracellular proteins, and necrotic cell debris [7]. Thus, macropinocytosis represents one of the main scavenging pathways that support cancer cell proliferation in low nutrient environment. In addition, it

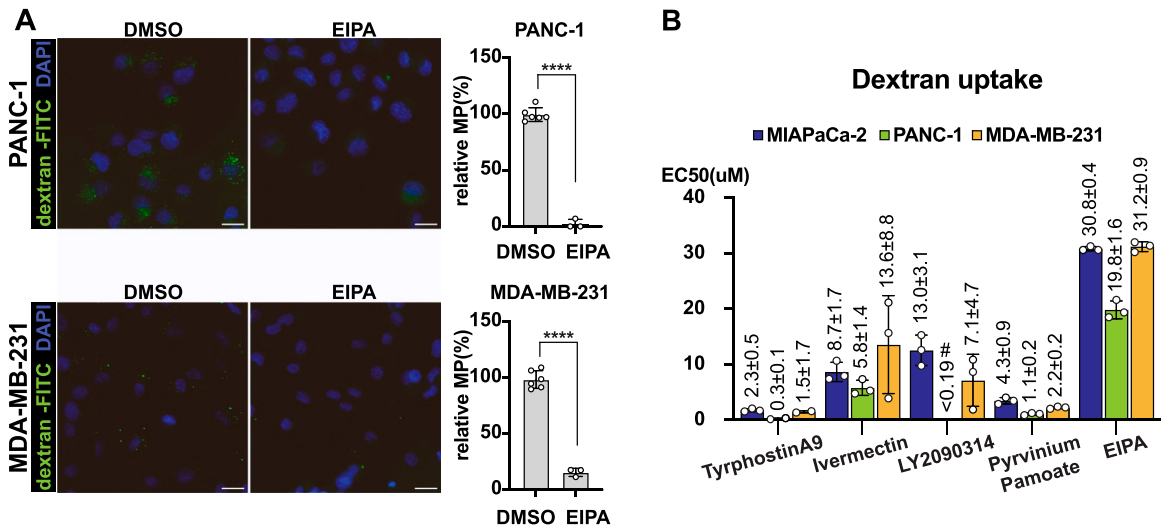

Fig. 6. :Performance of dextran uptake inhibition in different macropinocytic cell lines. (A) Representative images of dextran uptake assay on PANC-1 and MDA-MB-231 cells, respectively pancreatic and breast cancer cell lines. Cells were pre-incubated for 3 hours with DMSO or EIPA (75uM) prior to addition of dextran-FITC. Quantification of macropinocytosis was evaluated on SpotDensity parameter and is reported relative to the DMSO condition; data are reported as mean ± SD for n=6 (DMSO) or n=3 (EIPA) biological replicates with at least 400 cells scored per condition; ****p≤0.0001 by unpaired two-tailed Student's *t*-test. MP= macropinocytosis. Scale bar: 20 μm. (B) EC_{50} concentration for dextran uptake inhibition was obtained for the three cell lines, following SpotDensity parameter. Dose-response curves were obtained plotting inhibitors activity as percentage of dextran uptake relative to the DMSO control in each cell line; EC_{50} values were calculated using Prism software and are reported as mean ± SD, n=3 biological replicates (n=2 for Tryphostin A9 in PANC-1 and MDA-MD-231 cells). It was not possible to determine the EC_{50} value for the compound LY2090314 in PANC-1 cells, due to an inhibition greater than 50 % even at the lowest tested dose (0.19uM, #).

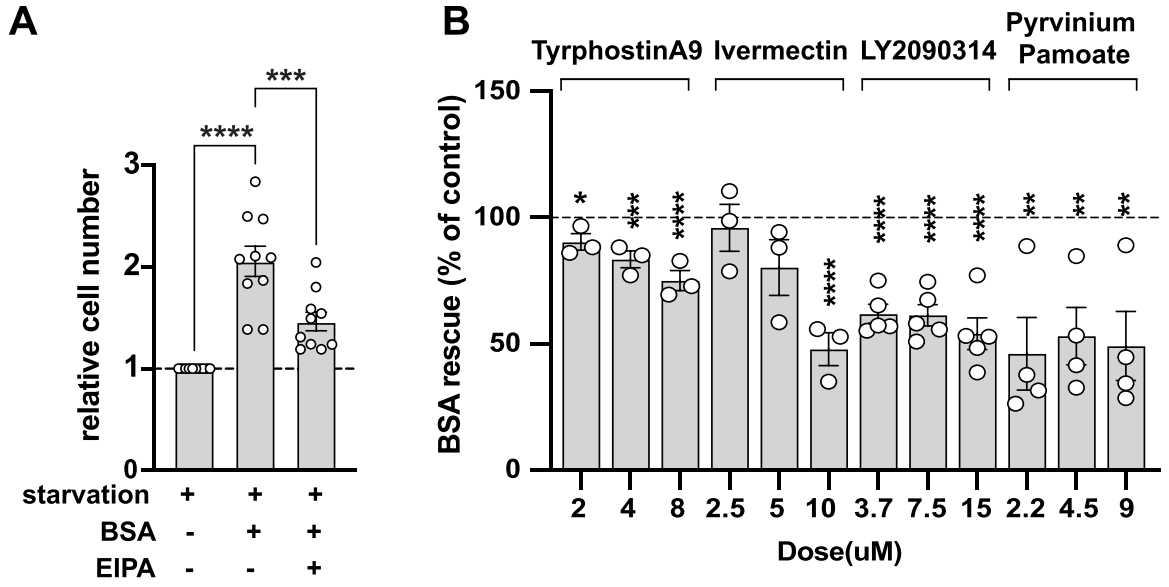

Fig. 7. :Inhibitors effect on BSA-dependent proliferation of PANC-1 cells. (A) Proliferation of PANC-1 cells after 96 h of growth in starvation conditions (low serum/low glutamine) ± 4 % BSA and EIPA (50uM). Data are reported as relative to the cell number at the beginning of starvation, on the day after seeding. Values are mean ± SEM of n=10 independent experiments performed in triplicates. ***p≤0.001, ****p≤0.0001 by one-way ANOVA with Bonferroni post-hoc test. (B) Effect of inhibitors on BSA-dependent proliferation during starvation in PANC-1 cells. Data are expressed as percentage of growth after 96 h compared to DMSO-treated cells in starvation +4 % BSA. Values are mean ±SEM of n≥3 independent experiments performed in triplicates. *p≤0.05, **p≤0.01, ***p≤0.001, ****p≤0.0001 by one-way ANOVA with Bonferroni post-hoc test; multiple comparisons for each inhibitor performed separately, relative to DMSO control.

has an important role in conferring resistance to different chemotherapeutics such as 5-Fluorouracil (5-FU), Gemcitabine, and Doxorobucin [10].

On these premises, targeting macropinocytosis has a clear therapeutic relevance and implies possible therapeutic benefits, limiting cancer cell growth and the eventual chemotherapeutics resistance [42]. Particularly PDAC, among other cancers, presents a unique tissue microenvironment characterized by dense fibrosis (desmoplasia) resulting in high interstitial pressure and low nutrient and oxygen diffusion. To survive and succeed in this peculiar and hostile environment, PDAC cells reprogram their metabolism and utilize scavenging pathways like macropinocytosis for metabolism homeostasis [24–26]. The relevance of this mechanism for the growth and thrive of PDAC led us to conduct the screening for the identification of novel and selective macropinocytosis inhibitors using MIAPaCa-2 cells, a well-known and characterized KRAS-mutated PDAC cancer cell line.

In our study, after optimizing a cell-based assay for high-content screening, we tested 3584 small molecules (including 989 FDA-

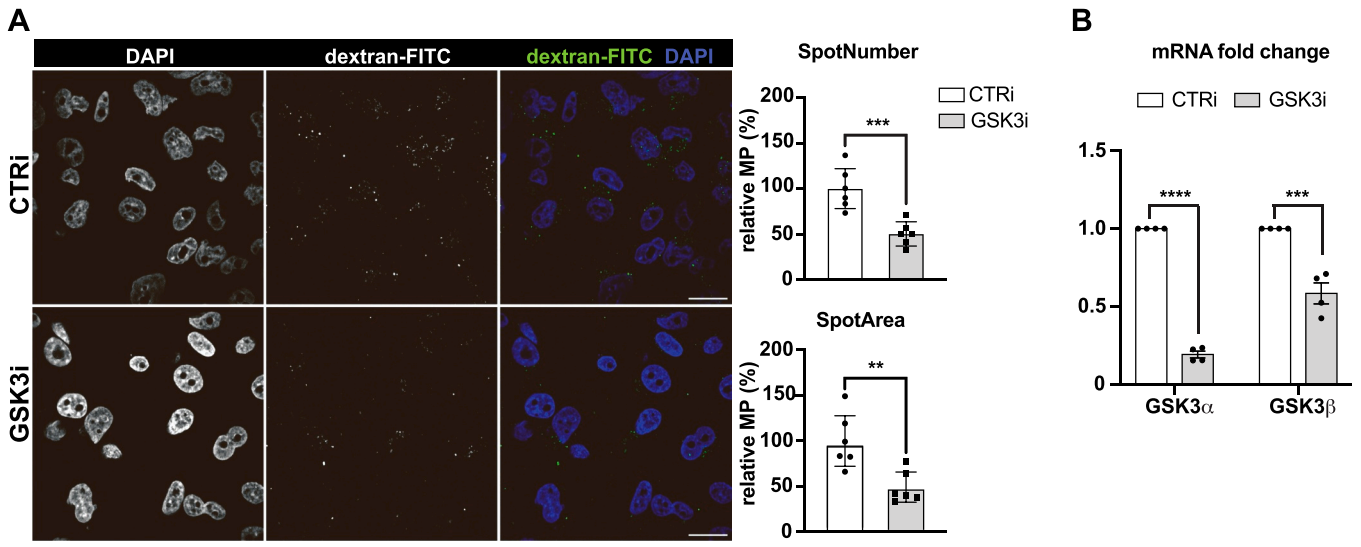

Fig. 8. :Impact of GSK3 interference on dextran uptake in MIAPaCa-2 cells. (A) Representative images of dextran-FITC uptake upon MIAPaCa-2 cells transfection with control or GSK3-siRNA. Quantification of macropinocytosis was performed using the 'Analyze Particles' feature in ImageJ, counting the total SpotNumber and the total SpotArea in a given field and dividing for the total cell nuclei in the corresponding field. Data are reported as relative to the control-siRNA condition; values are mean ± SD of n=6 biological replicates, with a minimum of 12 fields each; **p≤0.01, ***p≤0.001 by unpaired two-tailed Student's *t*-test. MP= macropinocytosis. Scale bar: 20 μm. (B) qRT-PCR analysis showing transcript levels for GSK3 α and β isoforms upon siRNA transfection. Data are reported as Calibrated Normalized Relative Quantity compared to control-siRNA. Values are mean ± SEM of n=4 biological replicates performed in triplicates. ***p≤0.001, ****p≤0.0001 by unpaired two-tailed Student's *t*-test.

approved drugs) for their ability to inhibit dextran internalization in MIAPaCa-2 cells.

The primary screening led to identify and select 18 small molecules that inhibited macropinosome-mediated dextran internalization. Subsequently, general endocytic inhibitors were identified through a Transferrin internalization assay and excluded from follow-up analysis. Thus, we selected 12 specific macropinocytosis inhibitors significantly more effective than EIPA, including: anticancer drugs such as Poziotinib and Tyrphostin A9 targeting EGFR and PDGFR respectively; anthelmintic drugs such as Pyrvinium Pamoate and Fenbendazole; natural products such as AvermectinA1a and its close analogue Ivermectin, marketed as an antiparasitic drug; and a GSK3 inhibitor (LY2090314). The reduced macropinocytic dextran uptake revealed after GSK3 downregulation, obtained by RNA interference, corroborated the data obtained with LY2090314, therefore suggesting that the effect of the small molecule could be ascribed to GSK3 inhibition rather than an off-target effect. Importantly, these data also suggest that the role of GSK3 in the macropinocytosis process could be cell-type specific and context -dependent.

The selected small molecules were additionally characterized looking at their ability to hamper the albumin-dependent MIAPaCa-2 cell growth under nutritionally limited conditions. A concurrent analysis conducted on BxPC-3 cells, a wild-type KRAS pancreatic cancer cell line, let to verify whether the uncovered effect was specific for KRAS-mutated cells. Indeed, we observed that just four small molecules (Tyrphostin A9, LY2090314, Ivermectin, and Pyrvinium Pamoate) out of the twelve tested showed a preferential effect on KRAS-mutated cancer cells. The inhibitory effects of these molecules on dextran uptake and albumin-dependent growth are not limited to MIAPaCa-2 cells but were also replicated in another pancreatic KRAS-mutated cancer cell line (PANC-1) and in triple negative breast cancer cells (MDA-MB-231). In the next future, it will be crucial to identify the molecular mechanisms by which the aforementioned inhibitors operate in order to fully leverage their therapeutic potential. In this context, our findings that GSK3 mediates macropinocytosis in MIAPaCa-2 cells suggest that the effects of the GSK3 inhibitor (LY2090314) may be due to its targeted activity.

In addition to the validation and characterization of the inhibitor compounds, during the screening five small molecules were also identified as inducers of macropinocytosis, among which three are marketed drugs: Digoxin, Levobunolol, and Colchicine. Of note, while in general cancer cells take advantage of macropinocytosis, its hyperactivation can elicit a non-apoptotic cell death, known as methuosis, characterized by the aberrant accumulation of macropinosomes and a consequent extreme cytoplasmatic vacuolization in some cancer types [15,43–45]. Future studies are worth to investigate the effect of the identified inducers in those cancer cells more susceptible to methuosis.

Ultimately, we tested the four selected inhibitors in a 3D cell culture system under nutrient-deprived conditions, focusing on their effects on cell growth and their ability to induce cell death. Tyrphostin A9, LY2090314, and Pyrvinium Pamoate all demonstrated a detrimental effect on the growth of spheroids and also caused a modest but significant increase in cell death, unlike what was observed for Ivermectin. Noticeably, all the drugs tested, including Ivermectin, negatively impacted the growth of the epithelial cancer component in the spheroids. EIPA and Tyrphostin A9 were particularly effective against the MIAPaCa-2 cells, suggesting they primarily target this cell type. However, we cannot rule out that the other drugs may also affect the Cancer-Associated Fibroblast (CAFs) component of the spheroids. This is significant, given that our 3D co-culture system is designed to more closely replicate the in vivo conditions of pancreatic tumors, where CAFs are known to support the macropinocytosis and overall viability of cancer epithelial cells [46,47].

Particularly noteworthy among the drugs effective in the 3D model is Pyrvinium Pamoate. This anthelmintic drug, as highlighted in recent research by Schultz et al. [48], has shown promise in inhibiting pancreatic cancer cells under nutrient-depleted conditions by targeting the mitochondria. Moreover and importantly, the initiation of a clinical trial to evaluate the safety and tolerability of Pyrvinium Pamoate in pancreatic cancer patients underscores an effective interest in repurposing Pyrvinium Pamoate for cancer therapy (ClinicalTrials.gov Identifier NCT05055323). Based on our findings, which demonstrate Pyrvinium Pamoate's effect on macropinocytosis, and considering the research by Schultz et al. [48], we speculate that the anthelmintic drug could simultaneously target two aspects of pancreatic cancer cell metabolism, under nutrient limiting conditions. This dual-action approach may enhance the drug's effectiveness against cancer cell

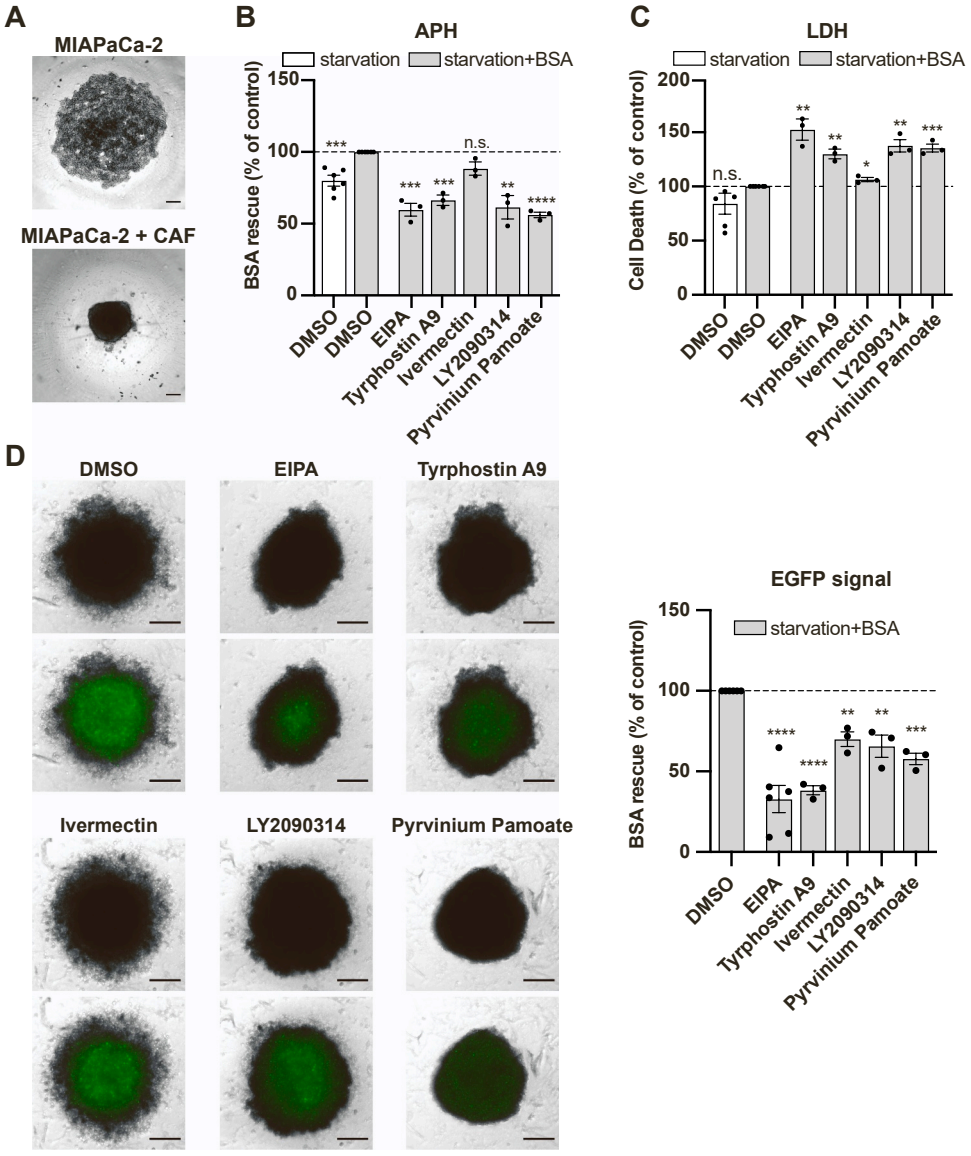

Fig. 9. :Effect of macropinocytosis inhibitors on organotypic 3D culture growth. (A) Representative images showing evident morphological differences of MIAPaCa-2 spheroids generated after 4 days in culture with or without Cancer Associated Fibroblasts (CAF). Brightfield images were taken at Operetta with 5x air objective. Scale bar: 200 μm. (B) Spheroids viability was assessed by Acid Phosphatase Assay (APH). Pre-formed spheroids were incubated with the inhibitors for 6 days, in starvation conditions (low serum/no glutamine) in the presence of BSA. To monitor the BSA-rescue effect, DMSO control in starvation without BSA supplementation was included (white bar). Data are expressed as compared to viability of DMSO control+BSA. (C) Spheroids cell death was assessed by Lactate Dehydrogenase (LDH) cytotoxicity assay. Upon inhibitors incubation as described in (B), a fraction of the supernatant was collected to measure the LDH protein release due to cell death. Data are expressed as compared to LDH release in DMSO control+BSA condition. In both panels values are mean ± SEM with n=6 (DMSO) or n=3 independent experiments with at least 3 technical replicates. *p≤0.05, **p≤0.01, ***p≤0.001 by unpaired two-tailed Student's *t*-test; n.s., not significant. (D) Representative images of spheroids generated with MIAPaCa-2 cells constitutively expressing H2B-EGFP marker and CAF cells. Images were taken in Brightfield and FITC channel at 5x, after 6 days of treatment as in (B) and (C). Quantification of total EGFP signal intensity is reported relative to the DMSO condition; data are reported as mean ± SD for minimum n=3 biological replicates; **p≤0.01, ***p≤0.001, ****p≤0.0001 by unpaired two-tailed Student's *t*-test. Scale bar: 200 μm.

growth, laying a foundation for its potential repurposing in cancer treatment.

Supplementary informations

Figure S1. Performance of candidate hits in the confirmation run of the screening campaign. Figure S2. Inactivity of a subset of dextran uptake inhibitors on BSA-dependent proliferation in MIAPaCa-2 cells. Table S1. Summary of the quantitative differential effects of selected compounds on BSA-dependent growth rescue presented in Fig. 4B and C.

Funding

We are grateful to Ravelli Family for the generous donation supporting Experimental Therapeutics Program activity. S.K.D. was supported by a fellowship kindly donated by R. Dal Zuffo in memory of Claudia, Allegra and Celeste Bordoni. This work was also supported in part by the following grant: ERC-Synergy (Grant# 101071470); AIRC-IG (Grant#22821); by the Italian Ministry of University and Research (Progetti di Rilevante Interesse Nazionale-PRIN, prot. 2022T9RM8) to G.S.

CRediT authorship contribution statement

Silvia Brambillasca: Investigation, Methodology, Formal analysis, Writing – original draft, Visualization. **Maria Rosaria Cera:** Investigation, Methodology, Formal analysis, Writing – review & editing, Visualization. **Adrian Andronache:** Software, Formal analysis, Data curation. **Sumit Kumar Dey:** Investigation, Formal analysis, Writing – review & editing. **Giovanni Fagá:** Investigation, Data curation. **Daniele Fancelli:** Resources, Data curation. **Emanuela Frittoli:** Supervision. **Maurizio Pasi:** Resources. **Michela Robusto:** Investigation, Data curation. **Mario Varasi:** Resources, Supervision. **Giorgio Scita:** Conceptualization, Writing – original draft, Founding acquisition. **Ciro Mercurio:** Conceptualization, Writing – original draft, Founding acquisition.

Declaration of Competing Interest

The authors declare that they have no competing interests.

Data availability

Data will be made available on request.

Acknowledgments

We thank members of the Experimental Therapeutics Program for helpful discussions; V. Dall'Olio and L. Tizzoni at Cogentech for qRT-PCR services.

Appendix A. Supporting information

Supplementary data associated with this article can be found in the online version at doi:10.1016/j.biopha.2024.116991.

References

[1] M.C. Kerr, R.D. Teasdale, Defining macropinocytosis, Traffic 10 (4) (2009) 364–371.
[2] J.A. Swanson, Shaping cups into phagosomes and macropinosomes, Nat. Rev. Mol. Cell Biol. 9 (8) (2008) 639–649.
[3] W. Palm, Metabolic functions of macropinocytosis, Philos. Trans. R. Soc. Lond. B Biol. Sci. 374 (1765) (2019) 20180285.
[4] R. Zeineddine, J.J. Yerbury, The role of macropinocytosis in the propagation of protein aggregation associated with neurodegenerative diseases, Front Physiol. 6 (2015) 277.
[5] S.A. Doodnauth, S. Grinstein, M.E. Maxson, Constitutive and stimulated macropinocytosis in macrophages: roles in immunity and in the pathogenesis of atherosclerosis, Philos. Trans. R. Soc. Lond. B Biol. Sci. 374 (1765) (2019) 20180147.
[6] C. Commisso, The pervasiveness of macropinocytosis in oncological malignancies, Philos. Trans. R. Soc. Lond. B Biol. Sci. 374 (1765) (2019) 20180153.
[7] B.T. Finicle, V. Jayashankar, A.L. Edinger, Nutrient scavenging in cancer, Nat. Rev. Cancer 18 (10) (2018) 619–633.
[8] C. Commisso, S.M. Davidson, R.G. Soydaner-Azeloglu, S.J. Parker, J.J. Kamphorst, S. Hackett, E. Grabocka, M. Nofal, J.A. Drebin, C.B. Thompson, J.D. Rabinowitz, C. M. Metallo, M.G. Vander Heiden, D. Bar-Sagi, Macropinocytosis of protein is an amino acid supply route in Ras-transformed cells, Nature 497 (7451) (2013) 633–637.
[9] S.M. Kim, T.T. Nguyen, A. Ravi, P. Kubiniok, B.T. Finicle, V. Jayashankar, L. Malacrida, J. Hou, J. Robertson, D. Gao, J. Chernoff, M.A. Digman, E.O. Potma, B.J. Tromberg, P. Thibault, A.L. Edinger, PTEN deficiency and AMPK activation promote nutrient scavenging and anabolism in prostate cancer cells, Cancer Discov. 8 (7) (2018) 866–883.
[10] V. Jayashankar, A.L. Edinger, Macropinocytosis confers resistance to therapies targeting cancer anabolism, Nat. Commun. 11 (1) (2020) 1121.
[11] E. Michalopoulou, F.R. Auciello, V. Bulusu, D. Strachan, A.D. Campbell, J. Tait-Mulder, S.A. Karim, J.P. Morton, O.J. Sansom, J.J. Kamphorst, Macropinocytosis renders a subset of pancreatic tumor cells resistant to mTOR inhibition, Cell Rep. 30 (8) (2020) 2729–2742, e4.
[12] H. Su, F. Yang, R. Fu, X. Li, R. French, E. Mose, X. Pu, B. Trinh, A. Kumar, J. Liu, L. Antonucci, J. Todoric, Y. Liu, Y. Hu, M.T. Diaz-Meco, J. Moscat, C.M. Metallo, A. M. Lowy, B. Sun, M. Karin, Cancer cells escape autophagy inhibition via NRF2-induced macropinocytosis, Cancer Cell 39 (5) (2021) 678–693, e11.
[13] B. King, J. Araki, W. Palm, C.B. Thompson, Yap/Taz promote the scavenging of extracellular nutrients through macropinocytosis, Genes Dev. 34 (19-20) (2020) 1345–1358.
[14] Y. Zhang, C. Commisso, Macropinocytosis in cancer: a complex signaling network, Trends Cancer 5 (6) (2019) 332–334.
[15] J.H. Overmeyer, A. Kaul, E.E. Johnson, W.A. Maltese, Active ras triggers death in glioblastoma cells through hyperstimulation of macropinocytosis, Mol. Cancer Res. 6 (6) (2008) 965–977.
[16] G. Redelman-Sidi, G. Iyer, D.B. Solit, M.S. Glickman, Oncogenic activation of Pak1-dependent pathway of macropinocytosis determines BCG entry into bladder cancer cells, Cancer Res. 73 (3) (2013) 1156–1167.
[17] M. Mettlen, A. Platek, P. Van Der Smissen, S. Carpentier, M. Amyere, L. Lanzetti, P. de Diesbach, D. Tyteca, P.J. Courtoy, Src triggers circular ruffling and macropinocytosis at the apical surface of polarized MDCK cells, Traffic 7 (5) (2006) 589–603.
[18] A. Veithen, P. Cupers, P. Baudhuin, P.J. Courtoy, v-Src induces constitutive macropinocytosis in rat fibroblasts, J. Cell Sci. 109 (Pt 8) (1996) 2005–2012.
[19] N. Tejeda-Munoz, L.V. Albrecht, M.H. Bui, E.M. De Robertis, Wnt canonical pathway activates macropinocytosis and lysosomal degradation of extracellular proteins, Proc. Natl. Acad. Sci. 116 (21) (2019) 10402–10411.
[20] G. Redelman-Sidi, A. Binyamin, I. Gaeta, W. Palm, C.B. Thompson, P.B. Romesser, S.W. Lowe, M. Bagul, J.G. Doench, D.E. Root, M.S. Glickman, The canonical wnt pathway drives macropinocytosis in cancer, Cancer Res. 78 (16) (2018) 4658–4670.
[21] S.W. Lee, Y. Zhang, M. Jung, N. Cruz, B. Alas, C. Commisso, EGFR-Pak signaling selectively regulates glutamine deprivation-induced macropinocytosis, Dev. Cell 50 (3) (2019) 381–392, e5.
[22] R.M. Perera, N. Bardeesy, Pancreatic cancer metabolism: breaking it down to build it back up, Cancer Discov. 5 (12) (2015) 1247–1261.
[23] C.J. Halbrook, C.A. Lyssiotis, Employing metabolism to improve the diagnosis and treatment of pancreatic cancer, Cancer Cell 31 (1) (2017) 5–19.
[24] J. Encarnacion-Rosado, A.C. Kimmelman, Harnessing metabolic dependencies in pancreatic cancers, Nat. Rev. Gastroenterol. Hepatol. 18 (7) (2021) 482–492.
[25] J.J. Kamphorst, M. Nofal, C. Commisso, S.R. Hackett, W. Lu, E. Grabocka, M. G. Vander Heiden, G. Miller, J.A. Drebin, D. Bar-Sagi, C.B. Thompson, J. D. Rabinowitz, Human pancreatic cancer tumors are nutrient poor and tumor cells actively scavenge extracellular protein, Cancer Res. 75 (3) (2015) 544–553.
[26] S.M. Davidson, O. Jonas, M.A. Keibler, H.W. Hou, A. Luengo, J.R. Mayers, J. Wyckoff, A.M. Del Rosario, M. Whitman, C.R. Chin, K.J. Condon, A. Lammers, K. A. Kellersberger, B.K. Stall, G. Stephanopoulos, D. Bar-Sagi, J. Han, J. D. Rabinowitz, M.J. Cima, R. Langer, M.G. Vander Heiden, Direct evidence for cancer-cell-autonomous extracellular protein catabolism in pancreatic tumors, Nat. Med. 23 (2) (2017) 235–241.
[27] J. Friedrich, W. Eder, J. Castaneda, M. Doss, E. Huber, R. Ebner, L.A. Kunz-Schughart, A reliable tool to determine cell viability in complex 3-d culture: the acid phosphatase assay, J. Biomol. Screen 12 (7) (2007) 925–937.
[28] C. Commisso, R.J. Flinn, D. Bar-Sagi, Determining the macropinocytic index of cells through a quantitative image-based assay, Nat. Protoc. 9 (1) (2014) 182–192.
[29] M. Koivusalo, C. Welch, H. Hayashi, C.C. Scott, M. Kim, T. Alexander, N. Touret, K. M. Hahn, S. Grinstein, Amiloride inhibits macropinocytosis by lowering submembranous pH and preventing Rac1 and Cdc42 signaling, J. Cell Biol. 188 (4) (2010) 547–563.
[30] A.I. Ivanov, Pharmacological inhibition of endocytic pathways: is it specific enough to be useful? Methods Mol. Biol. 440 (2008) 15–33.
[31] H. Suwa, T. Yoshimura, N. Yamaguchi, K. Kanehira, T. Manabe, M. Imamura, H. Hiai, M. Fukumoto, K-ras and p53 alterations in genomic DNA and transcripts of human pancreatic adenocarcinoma cell lines, Jpn J. Cancer Res 85 (10) (1994) 1005–1014.
[32] S. Verstovsek, R. Mesa, M. Talpaz, J.J. Kiladjian, C.N. Harrison, S.T. Oh, A. M. Vannucchi, R. Rampal, B.L. Scott, S.A. Buckley, A.R. Craig, K. Roman-Torres, J. O. Mascarenhas, Retrospective analysis of pacritinib in patients with myelofibrosis and severe thrombocytopenia, Haematologica 107 (7) (2022) 1599–1607.
[33] H.P. Lin, B. Singla, P. Ghoshal, J.L. Faulkner, M. Cherian-Shaw, P.M. O'Connor, J. X. She, E.J. Belin de Chantemele, G. Csanyi, Identification of novel macropinocytosis inhibitors using a rational screen of Food and Drug Administration-approved drugs, Br. J. Pharm. 175 (18) (2018) 3640–3655.
[34] X. Le, R. Cornelissen, M. Garassino, J.M. Clarke, N. Tchekmedyian, J.W. Goldman, S.Y. Leu, G. Bhat, F. Lebel, J.V. Heymach, M.A. Socinski, Poziotinib in non-small-cell lung cancer harboring HER2 Exon 20 insertion mutations after prior therapies: ZENITH20-2 trial, J. Clin. Oncol. 40 (7) (2022) 710–718.
[35] Y.H. Park, K.H. Lee, J.H. Sohn, K.S. Lee, K.H. Jung, J.H. Kim, K.H. Lee, J.S. Ahn, T. Y. Kim, G.M. Kim, I.H. Park, S.B. Kim, S.H. Kim, H.S. Han, Y.H. Im, J.H. Ahn, J. Y. Kim, J. Kang, S.A. Im, A phase II trial of the pan-HER inhibitor poziotinib, in patients with HER2-positive metastatic breast cancer who had received at least two prior HER2-directed regimens: results of the NOV120101-203 trial, Int. J. Cancer 143 (12) (2018) 3240–3247.
[36] K.M. Mayle, A.M. Le, D.T. Kamei, The intracellular trafficking pathway of transferrin, Biochim Biophys. Acta 1820 (3) (2012) 264–281.
[37] L.H. Wang, K.G. Rothberg, R.G. Anderson, Mis-assembly of clathrin lattices on endosomes reveals a regulatory switch for coated pit formation, J. Cell Biol. 123 (5) (1993) 1107–1117.
[38] T.A. Hill, C.P. Gordon, A.B. McGeachie, B. Venn-Brown, L.R. Odell, N. Chau, A. Quan, A. Mariana, J.A. Sakoff, M. Chircop, P.J. Robinson, A. McCluskey, Inhibition of dynamin mediated endocytosis by the dynoles–synthesis and functional activity of a family of indoles, J. Med. Chem. 52 (12) (2009) 3762–3773.

[39] W. Palm, Y. Park, K. Wright, N.N. Pavlova, D.A. Tuveson, C.B. Thompson, The utilization of extracellular proteins as nutrients is suppressed by mTORC1, Cell 162 (2) (2015) 259–270.
[40] L.V. Albrecht, N. Tejeda-Munoz, M.H. Bui, A.C. Cicchetto, D. Di Biagio, G. Colozza, E. Schmid, S. Piccolo, H.R. Christofk, E.M. De Robertis, GSK3 inhibits macropinocytosis and lysosomal activity through the wnt destruction complex machinery, Cell Rep. 32 (4) (2020) 107973.
[41] J. Kuen, D. Darowski, T. Kluge, M. Majety, Pancreatic cancer cell/fibroblast co-culture induces M2 like macrophages that influence therapeutic response in a 3D model, PLoS One 12 (7) (2017) e0182039.
[42] J. Puccini, M.A. Badgley, D. Bar-Sagi, Exploiting cancer's drinking problem: regulation and therapeutic potential of macropinocytosis, Trends Cancer 8 (1) (2022) 54–64.
[43] W.A. Maltese, J.H. Overmeyer, Methuosis: nonapoptotic cell death associated with vacuolization of macropinosome and endosome compartments, Am. J. Pathol. 184 (6) (2014) 1630–1642.
[44] S. Chi, C. Kitanaka, K. Noguchi, T. Mochizuki, Y. Nagashima, M. Shirouzu, H. Fujita, M. Yoshida, W. Chen, A. Asai, M. Himeno, S. Yokoyama, Y. Kuchino, Oncogenic Ras triggers cell suicide through the activation of a caspase-independent cell death program in human cancer cells, Oncogene 18 (13) (1999) 2281–2290.
[45] E. Silva-Pavez, P. Villar, C. Trigo, E. Caamano, I. Niechi, P. Perez, J.P. Munoz, F. Aguayo, V.A. Burzio, M. Varas-Godoy, A.F. Castro, M.I. Colombo, J.C. Tapia, CK2 inhibition with silmitasertib promotes methuosis-like cell death associated to catastrophic massive vacuolization of colorectal cancer cells, Cell Death Dis. 10 (2) (2019) 73.
[46] Y. Zhang, M.V. Recouvreux, M. Jung, K.M.O. Galenkamp, Y. Li, O. Zagnitko, D. A. Scott, A.M. Lowy, C. Commisso, Macropinocytosis in cancer-associated fibroblasts is dependent on CaMKK2/ARHGEF2 signaling and functions to support tumor and stromal cell fitness, Cancer Discov. 11 (7) (2021) 1808–1825.
[47] T. Zhang, Y. Ren, P. Yang, J. Wang, H. Zhou, Cancer-associated fibroblasts in pancreatic ductal adenocarcinoma, Cell Death Dis. 13 (10) (2022) 897.
[48] C.W. Schultz, G.A. McCarthy, T. Nerwal, A. Nevler, J.B. DuHadaway, M.D. McCoy, W. Jiang, S.Z. Brown, A. Goetz, A. Jain, V.S. Calvert, V. Vishwakarma, D. Wang, R. Preet, J. Cassel, R. Summer, H. Shaghaghi, Y. Pommier, S.A. Baechler, M. J. Pishvaian, T. Golan, C.J. Yeo, E.F. Petricoin, G.C. Prendergast, J. Salvino, P. K. Singh, D.A. Dixon, J.R. Brody, The FDA-approved anthelmintic pyrvinium pamoate inhibits pancreatic cancer cells in nutrient-depleted conditions by targeting the mitochondria, Mol. Cancer Ther. 20 (11) (2021) 2166–2176.